Cattania, C., McGuire, J. J., Collins, J. A. (2017): Dynamic triggering and earthquake swarms on East Pacific Rise transform faults. - *Geophysical Research Letters*, *44*, 2, pp. 702—710.

DOI: http://doi.org/10.1002/2016GL070857

AGU PUBLICATIONS

Geophysical Research Letters

RESEARCH LETTER
10.1002/2016GL070857

Key Points:
- We perform a systematic search for dynamic triggering on three transform faults located along the equatorial East Pacific Rise
- Fault segments with low seismic coupling and high rates of microseismicity are more sensitive to dynamic triggering
- Surface waves that produce the highest normal stress changes and the largest first strain invariant appear more effective at triggering

Supporting Information:
- Supporting Information S1

Correspondence to:
C. Cattania,
camcat@gfz-potsdam.de

Citation:
Cattania, C., J. J. McGuire, and J. A. Collins (2017), Dynamic triggering and earthquake swarms on East Pacific Rise transform faults, *Geophys. Res. Lett.*, *44*, 702–710, doi:10.1002/2016GL070857.

Received 16 AUG 2016
Accepted 23 NOV 2016
Accepted article online 6 DEC 2016
Published online 18 JAN 2017

Dynamic triggering and earthquake swarms on East Pacific Rise transform faults

Camilla Cattania[1,2], Jeffrey J. McGuire[2], and John A. Collins[2]

[1]GFZ German Research Center for Geosciences, Potsdam, Germany, [2]Woods Hole Oceanographic Institution, Woods Hole, Massachusetts, USA

Abstract While dynamic earthquake triggering has been reported in several continental settings, offshore observations are rare. Oceanic transform faults share properties with continental geothermal areas known for dynamic triggering: high geothermal gradients, high seismicity rates, and frequent swarms. We study dynamic triggering along the East Pacific Rise by analyzing 1 year of seismicity recorded by Ocean Bottom Seismographs. By comparing the response to teleseismic waves from global earthquakes, we find triggering to be most sensitive to changes in normal stress and to preferentially occur above 0.25 kPa. The clearest example of triggering occurs on the Quebrada and Gofar faults after the M_w8.0 Wenchuan earthquake. On Gofar, triggered seismicity occurs between the rupture areas of large earthquakes, within a zone characterized by aseismic slip, abundant microseismicity, frequent swarms, and low V_p. We infer that lithological properties inhibiting rupture propagation, such as high porosity and fluid content, also favor dynamic triggering.

1. Introduction

Dynamic stresses caused by seismic waves from remote earthquakes have been reported to trigger seismicity in several regions. With few exceptions [*Gonzalez-Huizar et al.*, 2012] observations have been confined to continental areas [e.g., *Brodsky*, 2000; *Prejean et al.*, 2004; *Brodsky and Prejean*, 2005; *Freed*, 2005], with transtensional areas being particularly sensitive [*Hill*, 2015; *Johnson and Bürgmann*, 2015]. While dynamic triggering is not restricted to a single tectonic environment [*Pankow et al.*, 2004; *Velasco et al.*, 2008; *Gonzalez-Huizar and Velasco*, 2011], vigorous triggered sequences have been recorded in areas with geothermal activity and volcanism [e.g., *Prejean et al.*, 2004; *Aiken and Peng*, 2014], suggesting that fluids play a role in the triggering mechanism.

Triggered earthquakes sometimes occur during the passage of the surface wave, directly due to the stress perturbation. Other times, an increase in seismicity rate has also been observed with a time delay, up to hours or days. The physical mechanism behind these events is debated. Within the framework of rate-state friction, the finite nucleation time of earthquakes can explain delayed triggering after a stress change [*Dieterich*, 1994], but numerical experiments indicate that near-instantaneous triggering is expected from passing surface waves [*Belardinelli*, 2003]. Delayed seismicity may be observed if surface waves trigger a prolonged creep event, which in turns triggers earthquakes [*Shelly et al.*, 2011].

The Quebrada/Discovery/Gofar (QDG) fault system is a set of transform faults in the East Pacific Rise (EPR), slipping at ~14 cm/yr. The faults have different seismic behavior. Gofar and Discovery present locked segments that periodically rupture in earthquakes with magnitudes between 5.5 and 6.2 [*McGuire*, 2008] as shown in Figure S1 in the supporting information. The spatially averaged seismic coupling on these faults is between 0.24 and 0.38 [*Wolfson-Schwehr*, 2015]. The rupture length of these events (~10 km) is smaller than the fault length, due to the presence of barriers that inhibit rupture propagation [*Roland et al.*, 2012]. These barriers are characterized by high rates of microseismicity, a reduction of 10–20% in *P* wave velocities [*Froment et al.*, 2014], and lower stress drops than nearby segments [*Moyer et al.*, 2016].

In contrast, the Quebrada fault rarely experiences $M_w \geq 5.5$ earthquakes, and most slip is accommodated aseismically: the seismic coupling here is <0.1 (Figure S1 in the supporting information). The presence of locked segments and rupture barriers of the Gofar and Discovery faults, and the comparison with the Quebrada fault provide a natural laboratory to study the sensitivity to dynamic triggering on faults with different degree of coupling and frictional behavior.

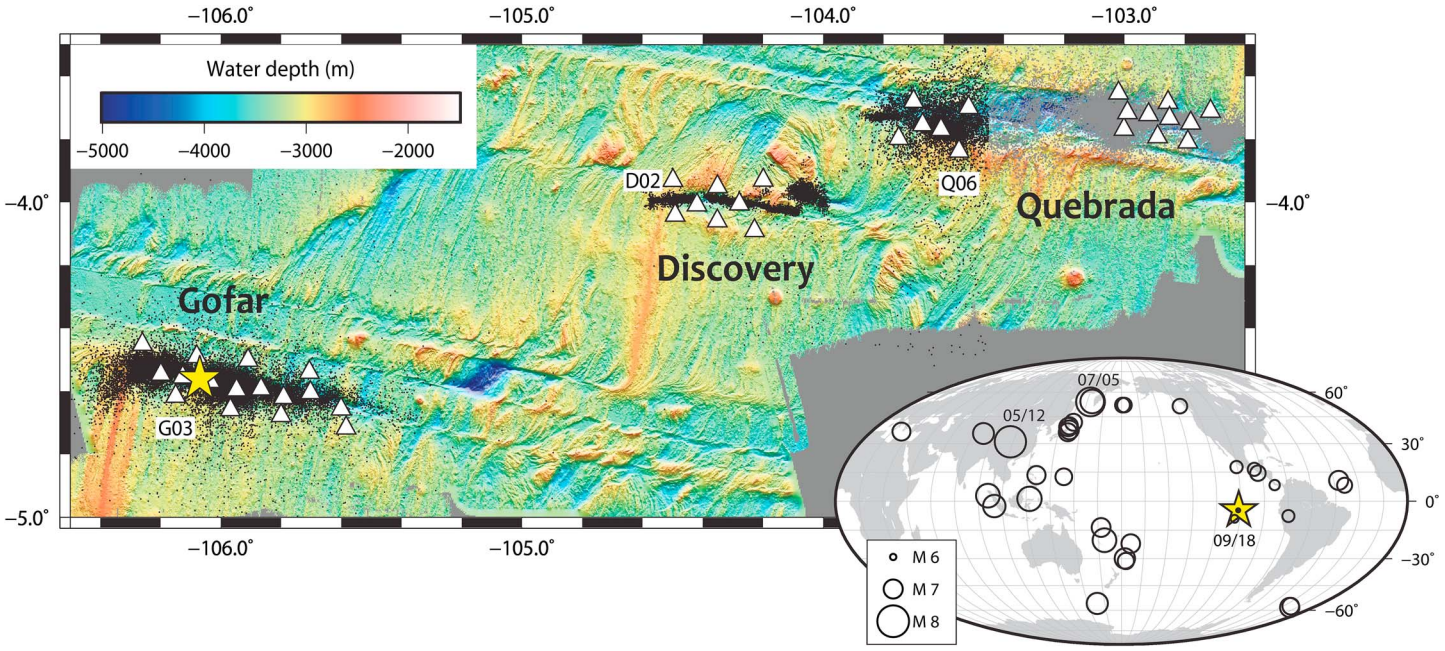

Figure 1. Seismicity recorded by Ocean Bottom Seismographs (OBSs) in 2008 (black/grey dots). For the Gofar and Quebrada faults, events from the STA/LTA catalog are shown: for Discovery, we show events relocated by *Wolfson-Schwehr et al.* [2014] with the hypoDD algorithm. Triangles are OBS locations. The grey dots in the central and east sections of Quebrada are not used in this study. The inset shows main shocks used as potential sources of dynamic triggering, from the global CMT catalog, with the date of events discussed in the text. The yellow star is the centroid of the M_w 6.0 earthquake on 18 September. Triangles indicate seismic stations, and those used for stress estimations are labeled.

2. Data and Methods

During 2008, the QDG fault system was monitored by 40 broadband and short-period Ocean Bottom Seismographs (OBSs; Figure 1). An array of 30 broadband OBSs allowed the detection of local high frequency events during the arrivals of large amplitude surface waves, ensuring that observed delay times are not an artifact due to an incomplete catalogue. The resulting data sets are described in section S1 of the Supplementary Material.

Dynamic triggering is associated with long period (15–30 s) surface waves [e.g., *Hill*, 2012]. Therefore, we search for dynamic triggering during and after the arrival of surface waves from events in the Global CMT catalogue. To account for the geometric spreading of surface waves, we select events with a seismic moment M_0 and a distance r such that the quantity M_0/r exceeds a threshold value (10^{15} J/km). For the Gofar fault we exclude the local $M_w = 6.0$ earthquake on 18 September and its $M_w = 5.3$ aftershock on the same day, since they are close enough to impose significant static stress changes. The resulting data sets comprise 36 events for the Gofar fault, 35 for Discovery, and 22 for Quebrada (Figure 1), listed in the supporting information.

Since aftershock sequences would also be detected as seismicity rate increases, we declustered the catalog using the method of *Reasenberg* [1985]. Increases in seismicity rates are indicated by high values in the β statistics, defined as

$$\beta(t, dt) = \frac{n(t, dt) - \dot{n}dt}{\sigma_n} \quad (1)$$

where $n(t, dt)$ is the number of events in the time window $[t-dt, t]$, $\dot{n}$ is the average rate, and σ_n is the standard deviation [*Matthews and Reasenberg*, 1988]. We do not constrain the duration and onset time of triggered seismicity, but we instead calculate β values for an array of times and time intervals [*Matthews and Reasenberg*, 1988]. We look for β anomalies within 15 h from the surface wave arrival, with respect to a background rate estimated on the previous 24 h. We verify that when choosing different time windows the same events present the highest β values, even though their ranking may change slightly. A common criterion for establishing the presence of triggered activity is $\beta \geq 2.0$. However, since we consider multiple times and durations, we find that this value is too low to be significant (it is exceeded more than 70% of the time for random 15 h intervals). We therefore use a threshold of $\beta = 4.5$ (which occurs about 20% of the time for random intervals).

Table 1. Global Earthquakes With β Anomalies Within 15 h From the Surface Wave Arrival[a]

Date	M_w	Distance (km)	β Time Delay (h)	β Duration (h)	ϵ^I (Nstrain)	ϵ^{II} (Nstrain^2)
			Gofar			
8 Feb	7.0	7311	2.0	2.0	1.5	6.5
14 Feb	6.9	13636	3.7	1.0	0.1	0.1
20 Mar	7.2	16494	2.0	13.0	1.2	3.5
7 May	6.9	12307	1.7	3.3	0.3	0.5
12 May	8.0	15762	3.0	11.3	8.2	202.2
30 Jun	7.0	9223	10.3	2.3	2.1	11.0
5 Jul	7.8	11139	13.7	1.3	1.6	57.5
30 Oct	6.1	542	7.7	5.7	3.3.	27.5
			Discovery			
14 Feb	6.9	13447	2.7	1.0	0.1	0.1
20 Mar	7.2	16453	10.0	1.0	1.2	3.3
2 May	6.7	9203	0.0	1.0	1.6	6.7
23 Jul	6.9	12327	6.7	1.0	0.8	1.5
10 Sep	6.9	7417	0.0	1.0	0.4	1.1
18 Sep	6.0	180	1.0	1.7	6.5	70.5
24 Sep	6.9	2398	9.7	1.0	2.8	17.9
16 Nov	6.7	14832	9.0	1.0	0.6	2.1
			Quebrada			
12 Feb	6.5	2465	10.3	1.7	1.5	1.1
3 Mar	6.9	14516	13.0	2.0	0.3	0.0
12 May	8.0	15888	8.7 (0.0)	5.7 (14.3)[b]	9.2	43.8
30 Jun	7.0	9145	5.7	1.0	1.7	1.6
5 Jul	7.8	11238	7.7 (5.7)	1.7 (4.3)[c]	1.3	0.9
18 Sep	6.0	283	4.3	4.3	4.5	10.2

[a]Background rates are calculated in the 24 h before the surface wave arrival. Distances are calculated from stations G03, D02, and Q06. The last two columns are the first and second strain tensor invariants.
[b]The values in brackets correspond to a secondary maximum in the β plot ($\beta = 4.98$).
[c]Another secondary maximum in the β plot ($\beta = 5.31$).

3. Results

We detect seismicity rate increases with $\beta \geq 4.5$ for 6–8 events on each fault (Table 1). β values following each main shock, and estimated peak dynamic stresses, are given in the supporting information. Calculating β values by testing a range of times and time intervals allows us to detect time windows with an elevated seismicity rate, without knowing their duration a priori. For an ideal case with elevated seismicity rates starting and ending abruptly, this method precisely identifies the duration of the anomaly. However, the results can be more ambiguous with real data, resulting in multiple maxima in the β plots. These are also reported in Table 2. In what follows, we summarize the most noteworthy observations for each fault.

3.1. Gofar

The surface wave from the M_w8.0 Wenchuan earthquake, which generated a peak Coulomb stress change of 1 kPa, was followed by an increase in seismicity rate (Figure 2). The β anomaly starts 3 h after the peak transient stress and lasts for more than 11 h. Delayed occurrence of β anomalies lasting few hours is also observed after the surface wave from several other earthquakes, including the second largest event (the M_w7.8 Kamchatka earthquake on 5 July), as summarized in Table 1.

We find that during β anomalies most earthquakes concentrate between latitude −105.9 and −106.0 (Figure 3), a region acting as a barrier to rupture propagation during large ($M_w \sim 6$) earthquakes [*McGuire et al.*, 2012]. We further describe the location of the swarm with respect to the fault's segmentation in the discussion section.

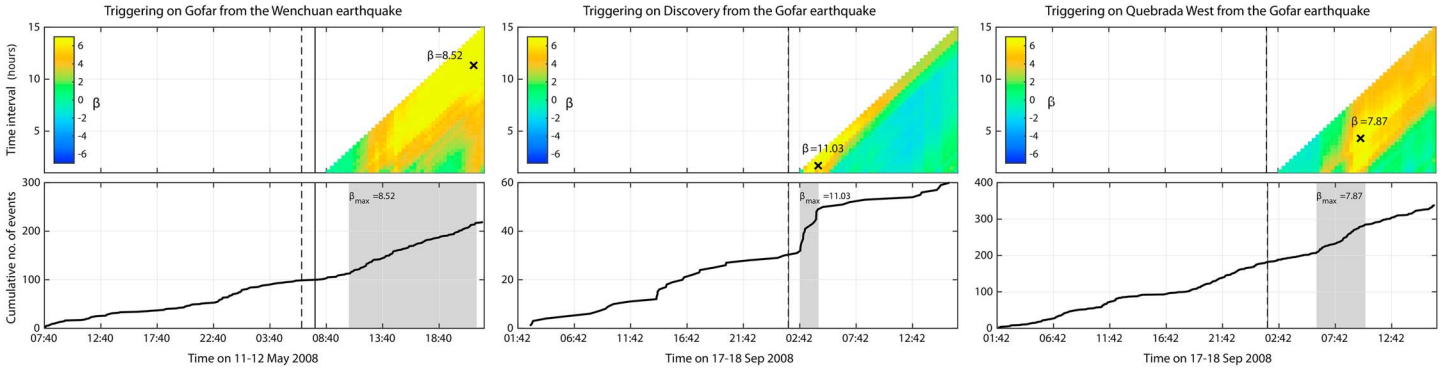

Figure 2. Examples of dynamic triggering on each fault. Top row is β plots: maxima of β indicate the time and duration of periods with high seismicity rate (shaded areas in bottom row). The dotted and continuous lines indicate the time of the remote earthquake and the surface wave arrival (peak in the vertical component of the waveform filtered at 0.01 – 0.05 Hz).

3.2. Discovery

The Discovery fault responded strongly to the M_w6.0 18 September earthquake on Gofar (Figure 2). A β anomaly of 11.03 starts ~1 h after the peak transient stress and lasts 1.7 h. Unlike β anomalies on Gofar and Quebrada, this swarm is not characterized by a constant seismicity rate over a few hours but by two short bursts, lasting about 20 and 1 min. The Gofar main shock is the smallest in magnitude and closest in distance among those analyzed. At a distance of 200 km, Discovery is approximately 20 fault lengths away from the earthquake, and triggering by static stress changes is unlikely.

We find several other instances of $\beta > 4.5$, with values up to 7.5. We note that these bursts tend to be shorter than those observed on Gofar and Quebrada, typically lasting 1 h (the smallest window length we tested). The Wenchuan earthquake, despite generating the largest stress changes on the fault (ΔCFS = 0.9 kPa), did not trigger seismicity.

3.3. Quebrada

Due to the station distribution (Figure 1), the completeness magnitude for Quebrada varies strongly in space; and therefore, we only consider seismicity west of longitude −103.45. Since the local catalog only covers up to 22 August, the data set of global earthquakes consists of 21 events. We find six instances of $\beta > 4.5$ (Table 1). Also in this case, an increase in seismicity rate is observed after the Wenchuan surface wave (ΔCFS = 0.6 kPa). The β anomaly starts 8.7 h after the surface wave, but an increase in activity can also be seen at the arrival of the surface wave from the Wenchuan earthquake, and lasts 14 h (giving a secondary maximum in the β plot). Additionally, we check if seismicity was triggered by the surface wave from the Gofar earthquake on 18 September by manually picking *P* and *S* wave arrivals for 48 h starting from 17 September 00:00:00 on station Q06 (Figure 1). We detect a β anomaly starting 4.3 h after the surface wave and lasting 4.3 h (Figure 2). We calculate local magnitudes and verify that the swarm is not an aftershock sequence.

4. Discussion

We performed a systematic search for dynamic triggering along the Gofar-Discovery-Quebrada fault system in the East Pacific Rise during 2008. We find that the two $M_w \geq 7.5$ earthquakes are followed by an increase in seismicity on the Gofar and the Quebrada faults, and the surface wave of the M_w6.0 Gofar earthquake triggers seismicity on the Discovery and the Quebrada faults.

Other examples of positive β anomalies during or shortly after the surface wave arrival are observed, and visual inspection of the seismograms reveals potentially triggered swarms. However, these observations are ambiguous due to the large number of similar swarms that are not triggered by remote seismic waves. We find that all three faults often experience seismic swarms leading to frequent β anomalies, even after declustering the catalog. In order to test the statistical significance of β anomalies as indicative of dynamic triggering, we need to verify how often they occur independently of incoming surface waves. We do so by drawing 500 random times during the year, using the same parameters described above (15 h search window and background rate calculated on the previous 24 h), from which we estimate the probability of obtaining $\beta \geq 4.5$ by chance. Given by the total number of $\beta \geq 4.5$ on Gofar in 2008, the probability of finding an anomaly in

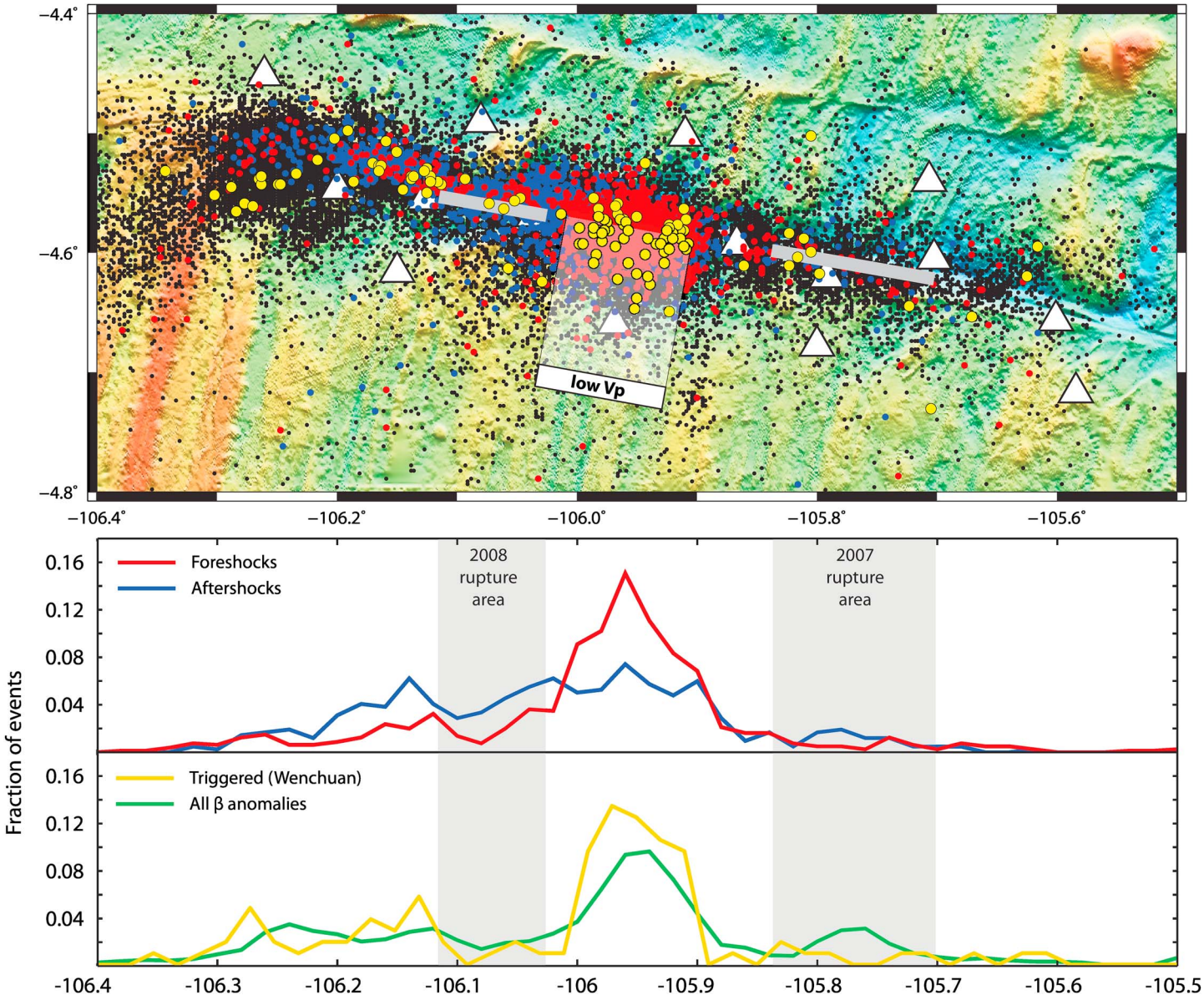

Figure 3. (top) Map view of seismicity along the Gofar fault, showing foreshocks of the 18 September M_w6.0 earthquake (10–18 September, in red), its aftershocks (18 September to 10 October, blue), and events triggered by the Wenchuan surface wave on 12 April (yellow). The grey lines are estimated rupture areas of the 18 September and the 2007 M_w6.0 earthquakes [*Wolfson-Schwehr et al.*, 2014; *Boettcher and Jordan*, 2004]. The shaded area is the low V_p area identified [*Roland et al.*, 2012; *Froment et al.*, 2014], offset from the fault for clarity. (bottom) Normalized spatial distributions of earthquakes along longitude. In addition to the events shown above, the green curve refers to all the swarms detected in 2008 ($\beta \geq 4.5$).

a 15 h window is 23%, and the chance of finding 8 or more anomalies out of 36 time windows is 61%. We performed the same test on the other faults: on Discovery, which has a similar rate of β anomalies as Gofar, the probability of at least 8 or more anomalies is 73%. On Quebrada, where fewer β anomalies are seen during the year, the probability of 5 anomalies out of 22 time windows is 36% (we did not include the anomaly from the Gofar earthquake in this estimation, since it was calculated using a different catalog). These results indicate that some of the β anomalies detected after incoming surface waves are probably not caused by them. The most robust examples of dynamic triggering are those that occur simultaneously on two faults: since the occurrence of a random β anomaly within 15 h on a given fault is about 20%, the occurrence of β anomalies on two faults in the same time window is only 4%. There are three common cases of triggering on both Quebrada and Gofar, two cases between Gofar and Discovery, and one case between Quebrada and Discovery (Table 1).

4.1. Factors Determining Occurrence of Dynamic Triggering

We investigated whether dynamic triggering preferentially occurs above a threshold in the transient stress or strain, by calculating strains imparted by the surface waves from the filtered (0.01–0.05 Hz) waveforms, at 5 km depth (see supporting information and *Hill* [2012]). We did not find evidence for a threshold or a correlation between β and any of following quantities: first and second strain invariants, shear stress and normal stress resolved on vertical faults with strike = 102°, Coulomb stress changes (with friction coefficient $\mu = 0.2, 0.6$), and azimuth. While a clear threshold cannot be inferred from the data, above $\Delta\sigma = 0.25$ kPa, β anomalies appear to be more frequent than on average and more than one standard deviation above the expected number of anomalies based on random chance. More specifically, Figure 4 (bottom) shows that the probability of finding the observed number of β anomalies by chance above a given $\Delta\sigma$ reaches a minimum ($p = 3\%$) at $\Delta\sigma = 0.25$ kPa. We find a similar pattern for ϵ^I, while the effect of shear stress seems less strong (Figure 4). These results suggest that dynamic triggering is most sensitive to volumetric and compressional stress changes. Other authors reported similar but higher stress thresholds, close to few kPa [e.g., *Brodsky and Prejean*, 2005; *Peng and Zhao*, 2009; *Aiken and Peng*, 2014]. The discrepancy can be due to the depth correction implicit in our stress calculations, and also to the fact that we are not defining an absolute threshold above which triggering always occurs, but a stress value above which seismicity rate increases is more frequent than usual.

4.2. Fault Properties Affecting Dynamic Triggering

On Gofar, the location of triggered seismicity in a rupture barrier provides some insight on the factors controlling sensitivity to dynamic triggering. The seismic behavior of this area has been recognized to differ from the adjacent segments during the foreshock-aftershock sequence of the M_w6.0 2008 earthquake [*McGuire et al.*, 2012]. A vigorous foreshock sequence took place here, and a drop in seismicity rate followed the main shock while aftershocks occurred in the adjacent segments. We find that most of the β anomalies occurring during the year (found by running the algorithm on the entire catalog) have similar durations and they are also located in this area (Figure 3). The occurrence of seismic swarms in barriers to rupture propagation due to along-strike variations in frictional properties has also been documented in subduction settings [*Holtkamp and Brudzinski*, 2014].

The low V_p in this segment [*Roland et al.*, 2012; *Froment et al.*, 2014] (Figure 3) indicates a highly damaged fault zone, with enhanced fluid circulation. The resistance to rupture propagation may be linked to the hydrological properties of this segment, including high porosity, the presence of velocity-strengthening hydrous phases, and a higher sensitivity to dilatancy [*McGuire et al.*, 2012]. Variations in fluid compressibility with effective stress have been suggested to control the seismic behavior of this region during different phases of the seismic cycle [*Géli et al.*, 2014]. The observation of dynamic triggering in areas with high fluid content is in agreement with previous reports from geothermal and volcanic settings. Dynamic triggering has been linked to high pore pressures, which enhances the fault sensitivity to small stress perturbations and promotes instantaneous triggering [e.g., *Brodsky and Prejean*, 2005]. In our case, however, the observed time delay between the surface wave and the onset of seismicity indicates that earthquakes are not triggered directly by stresses imparted by the wave but by an aseismic process triggered by stress transients. A plausible explanation is that the swarms are driven by slow slip events [*Shelly et al.*, 2011; *Peng et al.*, 2015], possibly facilitated by the presence of fluids and the effect of dilatancy [e.g., *Segall and Rice*, 1995]. These may sometimes take place spontaneously (as suggested by the concentration of "background" β anomalies in the rupture barrier on Gofar) and other times be triggered by dynamic stresses. Dynamic triggering of creep events is documented in geothermal areas [*Wei et al.*, 2015], although the estimated stress threshold (0.6 MPa) is orders of magnitude larger than the stresses recorded here.

Triggering takes place in the Gofar segment with the lowest nominal coupling (0.24 [*Wolfson-Schwehr*, 2015]). Note that this value is an average for the segment, and lower values are expected in the rupture barrier where triggering takes place. This area also experiences most of the swarms during the year (Figure 3), which may also be associated with fluids. The occurrence of triggering on the weakly coupled Quebrada during the surface wave of the Wenchuan earthquake also suggests that areas with low seismic coupling and high microseismicity are more prone to dynamic triggering.

The Discovery fault appears less sensitive to dynamic perturbations. In the analysis above, we showed that Discovery has the highest probability of the observed number of β anomalies being due to random chance, and β anomalies here tend to be shorter in duration. A more direct comparison of the three faults can be

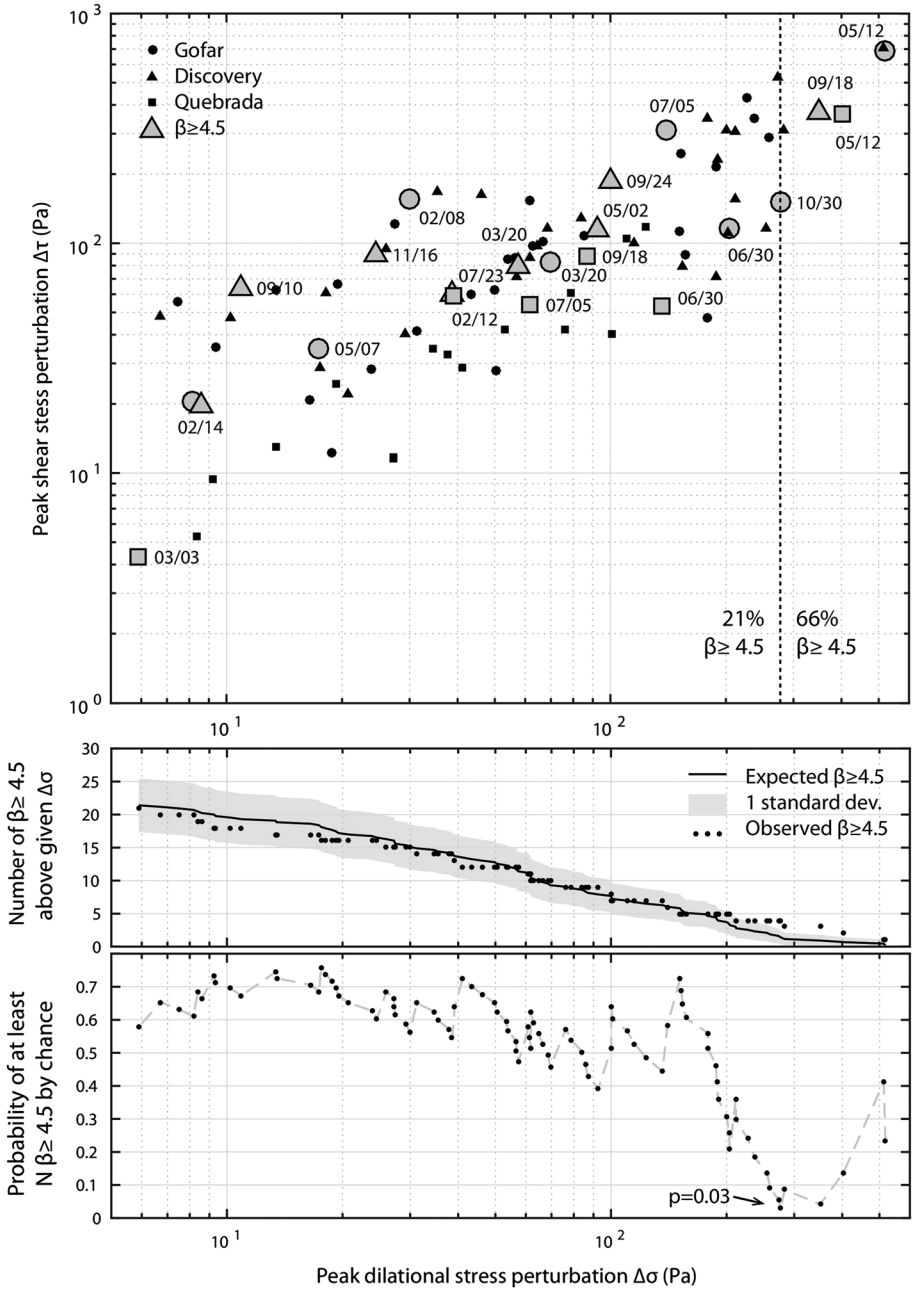

Figure 4. Top: maximum shear stress and normal stress change for all the candidate triggering earthquakes, on Gofar (triangles), Discovery (circles) and Quebrada West (squares). Large grey symbols indicate possible dynamic triggering (events that generated β anomalies $\geq$ 4.5). Strains are estimated from filtered (0.01-0.05 Hz) waveforms (see Supplementary Material). Middle: count of β anomalies above each stress threshold (black points), and expected number of β anomalies based on the rate of background β anomalies estimated from random time windows. This is the number of β anomalies expected by chance in N random time intervals, where N is the number of points with $\Delta\sigma \geq$ the stress values on the x axis. The grey area indicates one standard deviation. The count of β anomalies excludes the November 18th event, which falls outside the time period covered by the STA/LTA catalog. Bottom: probability that the observed number of β anomalies would occur by chance. Due to waveform quality, for Quebrada we only use the vertical component and thus neglect Love wave stresses: therefore, values may be underestimated.

made from their response to the surface wave from the Wenchuan earthquake, which imposed the highest stress perturbations on each fault, but only triggered seismicity on Gofar and Quebrada. We noted that seismicity triggered by this event was located in a low-coupling segment of Gofar, and on Quebrada. In contrast to these areas, most of Discovery (west of longitude −104.2) is more strongly coupled (coupling = 0.38 [*Wolfson-Schwehr*, 2015]). This suggests that the higher coupling on Discovery may be associated with less susceptibility to triggering.

However, Discovery reacted to the nearby M_w6.0 Gofar earthquake (Figure 2). This β anomaly lasted longer than the other anomalies on Discovery. This swarm is located on the edge of the eastern segment, with a lower coupling (0.26). The exact position in relation to past earthquake ruptures is not clear: seismicity is located on the eastern edge of the inferred rupture area of the 2012 M_w5.9 earthquake [*Wolfson-Schwehr et al.*, 2014], but due to uncertainties in the rupture length and centroid location, it is difficult to say whether they are within the locked zone or in the barrier.

5. Conclusions

We document possible instances of dynamic triggering on a set of transform faults on the East Pacific Rise. The M_w8.0 Wenchuan earthquake, which imparted the largest stresses on the faults, triggered earthquakes on Quebrada and on a barrier segment of Gofar, areas characterized by low seismic coupling. On Gofar, we find that the barrier segment frequently experiences swarms during the year. In both cases seismicity was triggered with a delay of few hours, indicating the occurrence of an aseismic process such as creep or fluid migration. A clear example of dynamic triggering on the Discovery fault occurs after the surface wave from the M_w6.0 Gofar earthquake. This and other potentially triggered swarms are shorter in duration on this fault than on the other two.

Due to presence of swarms in the area, care must be taken in interpreting other β anomalies. To this end, we calculate the rate of background swarms and estimated the probability of detecting them during the time windows in which we search for dynamic triggering. We find that β anomalies are more frequent than background swarms when the peak tensile normal stress calculated at 5 km depth exceeds a value of about 0.25 kPa.

Acknowledgments
We are grateful to Monica Wolfson-Schwehr for providing the relocated catalog and rupture lengths for Discovery and to Pamela Moyer for magnitude estimations for Gofar. C.C. was supported by the WHOI SSF program, a GeoSim Career Support fellowship and USGS award G14AP00058. The CMT global earthquake catalog can be accessed at http://www.globalcmt.org/CMTsearch.html. OBS data are available through the IRIS Data Management Center at http://ds.iris.edu/ds/nodes/dmc/.

References

Aiken, C., and Z. Peng (2014), Dynamic triggering of microearthquakes in three geothermal/volcanic regions of California, *J. Geophys. Res. Solid Earth*, *119*, 6992–7009, doi:10.1002/2014JB011218.

Aki, K., and P. G. Richards (1980), *Quantitative Seismology: Theory and Methods*, W. H. Freeman, New York.

Belardinelli, M. E. (2003), Earthquake triggering by static and dynamic stress changes, *J. Geophys. Res.*, *108*(B3), 2135, doi:10.1029/2002JB001779.

Boettcher, M. S., and T. H. Jordan (2004), Earthquake scaling relations for mid-ocean ridge transform faults, *J. Geophys. Res.*, *109*, B12302, doi:10.1029/2004JB003110.

Brodsky, E. E. (2000), A new observation of dynamically triggered regional seismicity: Earthquakes in Greece following the August, 1999 Izmit, Turkey earthquake, *Geophys. Res. Lett.*, *27*(17), 2741–2744, doi:10.1029/2000GL011534.

Brodsky, E. E., and S. G. Prejean (2005), New constraints on mechanisms of remotely triggered seismicity at Long Valley Caldera, *J. Geophys. Res.*, *110*, B04302, doi:10.1029/2004JB003211.

Dieterich, J. H. (1994), A constitutive law for rate of earthquake production and its application to earthquake clustering, *J. Geophys. Res.*, *99*(B2), 2601–2618.

Freed, A. M. (2005), Earthquake triggering by static, dynamic, and postseismic stress transfer, *Annu. Rev. Earth Planet. Sci.*, *33*, 335–367, doi:10.1146/annurev.earth.33.092203.122505.

Froment, B., J. J. McGuire, R. D. van der Hilst, P. Gouedard, E. C. Roland, H. Zhang, and J. A. Collins (2014), Imaging along-strike variations in mechanical properties of the Gofar transform fault, East Pacific Rise, *J. Geophys. Res. Solid Earth*, *119*, 7175–7194, doi:10.1002/2014JB011270.

Géli, L., J.-M. Piau, R. Dziak, V. Maury, D. Fitzenz, Q. Coutellier, P. Henry, D. Broseta, M. Steele-MacInnis, and T. Driesner (2014), Seismic precursors linked to super-critical fluids at oceanic transform faults, *Nat. Geosci.*, *7*(10), 757–761, doi:10.1038/ngeo2244.

Gonzalez-Huizar, H., and A. A. Velasco (2011), Dynamic triggering: Stress modeling and a case study, *J. Geophys. Res.*, *116*, B02304, doi:10.1029/2009JB007000.

Gonzalez-Huizar, H., A. A. Velasco, Z. Peng, and R. R. Castro (2012), Remote triggered seismicity caused by the 2011, *M*9.0 Tohoku-Oki, Japan earthquake, *Geophys. Res. Lett.*, *39*, L10302, doi:10.1029/2012GL051015.

Hill, D. P. (2012), Dynamic stresses, Coulomb failure, and remote triggering-corrected, *Bull. Seismol. Soc. Am.*, *102*(6), 2313–2336, doi:10.1785/0120120085.

Hill, D. P. (2015), On the sensitivity of transtensional versus transpressional tectonic regimes to remote dynamic triggering by Coulomb failure, *Bull. Seismol. Soc. Am.*, *105*(3), 1339–1348, doi:10.1785/0120140292.

Holtkamp, S., and M. R. Brudzinski (2014), Megathrust earthquake swarms indicate frictional changes which delimit large earthquake ruptures, *Earth Planet. Sci. Lett.*, *390*, 234–243, doi:10.1016/j.epsl.2013.10.033.

Johnson, C. W., and R. Bürgmann (2015), Delayed dynamic triggering: Local seismicity leading up to three remote M ≥ 6 aftershocks of the 11 April 2012 *M*8.6 Indian Ocean earthquake, *J. Geophys. Res. Solid Earth*, *121*, 134–151, doi:10.1002/2015JB012243.

Matthews, V., and A. Reasenberg (1988), Statistical methods for investigating quiescence and other temporal seismicity patterns, *Pure Appl. Geophys.*, *126*(2–4), 357–372, doi:10.1007/BF00879003.

McGuire, J. J. (2008), Seismic cycles and earthquake predictability on East Pacific Rise transform faults, *Bull. Seismol. Soc. Am.*, *98*(3), 1067–1084, doi:10.1785/0120070154.

McGuire, J. J., J. A. Collins, P. Gouédard, E. Roland, D. Lizarralde, M. S. Boettcher, M. D. Behn, and R. D. Van der Hilst (2012), Variations in earthquake rupture properties along the Gofar transform fault, East Pacific Rise, *Nat. Geosci.*, *5*(5), 336–341, doi:10.1038/ngeo1454.

Moyer, P. A., M. S. Boettcher, and J. J. McGuire (2016), Variations in earthquake source complexity and stress drop in rupture patches and rupture barriers on Gofar transform fault, East Pacific Rise, Abstract S13A-2517 presented at 2016 Fall Meeting, AGU, San Francisco, Calif., 12–16 Dec.

Pankow, K. L., W. J. Arabasz, J. C. Pechmann, and S. J. Nava (2004), Triggered seismicity in Utah from the 3 November 2002 Denali fault earthquake, *Bull. Seismol. Soc. Am.*, *94*(6), 332–347.

Peng, Z., and P. Zhao (2009), Migration of early aftershocks following the 2004 Parkfield earthquake, *Nat. Geosci.*, *2*(12), 877–881, doi:10.1038/ngeo697.

Peng, Z., D. R. Shelly, and W. L. Ellsworth (2015), Delayed dynamic triggering of deep tremor along the Parkfield-Cholame section of the San Andreas Fault following the 2014 *M*6.0 South Napa earthquake, *Geophys. Res. Lett.*, *42*, 7916–7922, doi:10.1002/2015GL065277.

Prejean, S. G., D. P. Hill, E. E. Brodsky, S. E. Hough, M. J. S. Johnston, S. D. Malone, D. H. Oppenheimer, A. M. Pitt, and K. B. Richards-dinger (2004), Remotely triggered seismicity on the United States West Coast following the *Mw* 7.9 Denali fault earthquake, *Bull. Seismol. Soc. Am.*, *94*(6B), S348–S359.

Reasenberg, P. (1985), Second-order moment of central California seismicity, 1969–1982, *J. Geophys. Res.*, *90*(B7), 5479–5495, doi:10.1029/JB090iB07p05479.

Roland, E., D. Lizarralde, J. J. McGuire, and J. A. Collins (2012), Seismic velocity constraints on the material properties that control earthquake behavior at the Quebrada-Discovery-Gofar transform faults, East Pacific Rise, *J. Geophys. Res.*, *117*, B11102, doi:10.1029/2012JB009422.

Segall, P., and J. R. Rice (1995), Dilatancy, compaction, and slip instability of a fluid-infiltrated fault, *J. Geophys. Res.*, *100*, 155–171.

Shelly, D. R., Z. Peng, D. P. Hill, and C. Aiken (2011), Triggered creep as a possible mechanism for delayed dynamic triggering of tremor and earthquakes, *Nat. Geosci.*, *4*(6), 384–388, doi:10.1038/ngeo1141.

Velasco, A. A., S. Hernandez, T. O. M. Parsons, and K. Pankow (2008), Global ubiquity of dynamic earthquake triggering, *Nat. Geosci*, 375–379, doi:10.1038/ngeo204.

Wei, M., Y. Liu, Y. Kaneko, J. J. McGuire, and R. Bilham (2015), Dynamic triggering of creep events in the Salton Trough, Southern California by regional $M > 5.4$ earthquakes constrained by geodetic observations and numerical simulations, *Earth Planet. Sci. Lett.*, *427*, 1–10, doi:10.1016/j.epsl.2015.06.044.

Wiemer, S. (2000), Minimum magnitude of completeness in earthquake catalogs: Examples from Alaska, the Western United States, and Japan, *Bull. Seismol. Soc. Am.*, *90*(4), 859–869, doi:10.1785/0119990114.

Wolfson-Schwehr, M. (2015), The relationship between oceanic transform fault segmentation, seismicity, and thermal structure, PhD thesis, University of New Hampshire, Durham, N. H.

Wolfson-Schwehr, M., M. S. Boettcher, J. J. McGuire, and J. A. Collins (2014), The relationship between seismicity and fault structure on the Discovery transform fault, East Pacific Rise, *Geochem. Geophys. Geosyst.*, *15*, 3698–3712, doi:10.1002/2014GC005445.